Frequency Response Bound Determination Using a Kharitonov and Algorithmic Framework

M. Sami Fadali
Electrical Engineering
University of Nevada
Reno, NV 89557
fadali@ee.unr.edu

L. LaForge
The Right Stuff
3341 Adler Court
Reno, NV 89503
larry@The-Right-Stuff.com

Frederick C. Harris, Jr.
Computer Science
University of Nevada
Reno, NV 89557
fredh@cs.unr.edu

Abstract

This paper uses Kharitonov stability theory and the theory of algorithms to efficiently compute frequency response bounds for control system design. We limit the analysis to the simple case of a plant transfer function with denominator uncertainty to gain insight into the determination of tracking, robust stability, and actuator bounds. A coordinate transformation allows us to reduce the computational time for the problem. We divide the compensator plane into separate regions with each region sharing the critical points of a value set needed in the computation of frequency response bounds. Our analysis demonstrates the importance of estimating asymptotic bounds on computational time as is standard in algorithmic analysis. We apply our algorithms to a two-simple examples.

I. Introduction

In quantitative feedback theory (QFT), the frequency domain design of control systems is accomplished by robustly satisfying a set of performance inequality constraints. QFT and related methodologies provide an integrated design procedure to satisfy tracking, robust stability, actuator, sensitivity, and other performance constraints in the presence of parameter uncertainty. As originally proposed, QFT required extensive experience to obtain good results [1]. Today, computer programs have made it accessible to the average control engineer [2]. However, the computational cost of determining feasible compensators becomes prohibitive as the number of uncertain parameters increases.

Several researchers have developed useful algorithms to reduce the time required to calculate the bounds used in QFT design [3], [4], [5], [6], [7]. In [3], the authors use value sets known from Kharitonov stability theory [8] to compute the tracking bounds for affine uncertainty in the numerator and denominator. In [4], QFT bounds are expressed as quadratic constraints to simplify their determination. Longdon and East [5] provide a geometrical technique for bound computation with the transfer function value set approximated by a polygon. It is well known that the value set of an affine polynomial is a polygon and the approach they provide can give only sufficient conditions for satisfying the design constraints.

Fadali and LaForge [6] introduced the notation and tools of algorithmic analysis to the computation of QFT bounds. The analysis was restricted to the simple case of a system with denominator uncertainty and a numerator known with arbitrary accuracy. In [7], Fadali and LaForge give optimal algorithms for computing QFT bounds for interval numerator and denominator polynomials. These two papers demonstrate that to assess the relative usefulness of newly proposed algorithms, it is essential to obtain asymptotic bounds on their computational time and to formally prove their correctness as is standard practice in algorithmic design.

The authors of [3] and [5] observed that the magnitude of the sum of a test compensation value (complex number) and a plant value set is the distance between the value set and the negative of the compensation value. This observation is the key to significant computational savings. For example, the upper bound on the closed loop frequency response (stability robustness bound) can be calculated by determining the minimum distance to a value set. Lower bound computation can be calculated by determining the maximum distance to a value set. The classical ratio tracking bound for QFT is an upper bound on the ratio of the maximum distance to the minimum distance to the value set.

In this paper, we further examine the simple problem solved in [6] and exploit the same observation. We show that in special cases the complex plane can be divided into regions where the farthest and closest points of the value set remain unchanged. A coordinate transformation simplifies the evaluation of both the stability robustness and tracking bounds by reducing the problem to one where the bounds are symmetric about the value set. The inverse transformation yields the required bounds, and the entire computation is achieved in constant time. These concepts are explained in this paper and demonstrated using two simple examples.

This paper is organized as follows: First, we examine the tracking and stability robustness bounds for a system with interval denominator uncertainty. Next, we introduce the coordinate transformation that simplifies the computation of the required QFT bounds and show that the complex plane can be divided into twelve regions (three when symmetry is considered) each of which has a fixed farthest and closest point in the rectangular value set. We then discuss the computational time [9] of the new algorithm as compared to [6] and to the standard gridding approach [2], [10]. Finally, we apply the new concepts to two simple examples.

II. Frequency Response Bounds

Consider a single-input-single-output system comprised of a plant and a feedback compensator. The closed-loop transfer function (CLTF) for the system is given by

$$|T(\omega)| = 1 \Big/ |P^{-1}(j\omega, p, q) + K(j\omega)| \tag{1}$$

where P is the uncertain plant transfer function, K is a compensator transfer function, and p and q are vectors of uncertain parameters for the numerator and denominator polynomials, respectively. We now discuss some design bounds commonly used in the literature. For a more complete account of these and other bounds, the reader is referred to the literature on QFT [1], [2].

Because we are primarily interested in the development of new computational tools for frequency response bounds, we focus our attention on the simplest meaningful problem for which those tools can be explored. We consider the case of a plant transfer function with denominator uncertainty

$$P(j\omega, p, q) = N(j\omega)/D(j\omega, q) \tag{2}$$

The maximum CLTF magnitude is therefore given by

$$|T(\omega)|_{\max} = |N(j\omega)| \Big/ \min_q |D(j\omega, q) + KN(j\omega)| \tag{3}$$

and the minimum CLTF magnitude is

$$|T(\omega)|_{\min} = |N(j\omega)| \Big/ \max_q |D(j\omega, q) + KN(j\omega)| \tag{4}$$

The worst-case magnitude ratio is

$$\frac{|T(\omega)|_{\max}}{|T(\omega)|_{\min}} = \frac{\max_q |D(j\omega,q) + KN(j\omega)|}{\min_q |D(j\omega,q) + KN(j\omega)|} \tag{5}$$

Let $C = x_c + j\, y_c$ be the product of K and N and rewrite (5) as

$$\frac{|T(\omega)|_{\max}}{|T(\omega)|_{\min}} = \frac{\max_q |D(j\omega,q) + C(j\omega)|}{\min_q |D(j\omega,q) + C(j\omega)|} \tag{6}$$

It will be convenient to rewrite (6) in the form

$$\frac{|T(\omega)|_{\max}}{|T(\omega)|_{\min}} = \frac{\max_q |D(j\omega,q) - C_m(j\omega)|}{\min_q |D(j\omega,q) - C_m(j\omega)|} \tag{7}$$

where $C_m = -C = (-x_c, -y_c) = (x, y)$. We now observe that the magnitudes in (3)-(7) involve distances between the values of the complex number D and the complex number C_m [3]. Thus, determining QFT tracking bounds is equivalent to determining the ratio of the maximum to minimum distance between the point C_m and the set D.

In addition, robust stability requires satisfying

$$|T(\omega)|_{\max} = \frac{|N(j\omega)|}{\min_q |D(j\omega, q) - C_m|} \le M_p, M_p > 0 \tag{8}$$

i.e.

$$\min_q |D(j\omega, q) - C_m| \ge \frac{|N(j\omega)|}{M_p} \tag{9}$$

For cascade compensation, (7) is unchanged, but the right hand side of (9) is multiplied by $|K|$. Similarly, the lower bound

$$|T(\omega)|_{mi} = \frac{|N(j\omega)|}{\min_q |D(j\omega, q) - C_m|} \ge M_l, M_l > 0 \tag{10}$$

is equivalent to the condition

$$\min_q |D(j\omega, q) - C_m| \le \frac{|N(j\omega)|}{M_l} \tag{11}$$

The tracking bound (7) yields an upper bound similar to (8) and a lower bound similar to (10). However, the computation of (8) and (10) is simpler. Furthermore, it is identical with the constant M_p and M_l used for (8) and (10), respectively. In later sections we use M_{lp} to denote either constant as we discuss our computational procedure.

Let D be the nth order interval polynomial

$$D(s; q) = a_n(q)\, s^n + a_{n-1}(q)\, s^{n-1} + \ldots + a_0(q) \tag{12}$$

with uncertainty bounds $a_i \in \left[a_i^-, a_i^+\right]$, $i = 0, 1, \ldots, n$. Then the value set associated with the uncertain polynomial is the Kharitonov rectangle $D^{\square}$ with generating polynomials [8]

$$\begin{aligned} D^{++}(s) &= a_0^+ + a_1^+ s + a_2^- s^2 + a_3^- s^3 + \cdots \\ D^{+-}(s) &= a_0^+ + a_1^- s + a_2^- s^2 + a_3^+ s^3 + \cdots \\ D^{-+}(s) &= a_0^- + a_1^+ s + a_2^+ s^2 + a_3^- s^3 + \cdots \\ D^{--}(s) &= a_0^- + a_1^- s + a_2^+ s^2 + a_3^+ s^3 + \cdots \end{aligned} \tag{13}$$

Refer to Figure 1; $(x, y) \in D^{\square}$ if and only if

$$x_- \le x \le x_+,\ y_- \le y \le y_+ \tag{14}$$

where x_+ (*resp.* x_-) denotes the real component of D^{++} (*resp.* D^{--}) and y_+ (*resp.* y_-) denotes the imaginary component of D^{++} (*resp.* D^{--}).

We show that the maximum and minimum magnitude corresponds either to an extreme point of the value set $D^{\square}$ or to a point on an edge of $D^{\square}$. Algorithmic computation of the minimum magnitude, maximum magnitude, and worst-case ratio is now tractable.

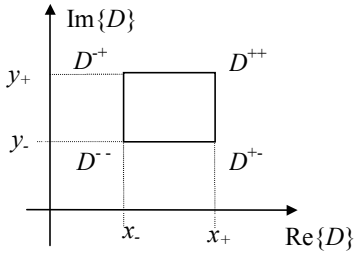

Fig. 1 Kharitonov rectangle $D^{\square}$.

III. Coordinate Transformation and the Maximum and Minimum Distance

To determine the stability robustness and tracking bounds for a system with denominator uncertainty, we obtain the maximum and minimum distances between a

test point $C_m = (x, y)$ and the Kharitonov rectangle $D^{\square}$. We use the notation

$$(x_{av}, y_{av}) = \left(\frac{x_- + x_+}{2}, \frac{y_- + y_+}{2} \right) \tag{15}$$

The plane can be divided into 12 regions. Within region *i,* there is a unique point $(\hat{x}, \hat{y}) \in D^{\square}$ at maximum distance from C_m and a unique point $(\breve{x}, \breve{y}) \in D^{\square}$ at minimum distance. We do not consider the interior of the Kharitonov rectangle since it corresponds to unstable systems.

Before we show the results of dividing the plane into regions, we discuss a coordinate transformation to reduce the subdivision of the complex plane for compensation boundary calculation to one where we have symmetry that can be exploited to reduce computation. We transform the compensation to (x, y) using

$$\begin{bmatrix} x \\ y \end{bmatrix} = -\begin{bmatrix} x_c \\ y_c \end{bmatrix} - \begin{bmatrix} x_{av} \\ y_{av} \end{bmatrix} \leftrightarrow \begin{bmatrix} x_c \\ y_c \end{bmatrix} = -\begin{bmatrix} x \\ y \end{bmatrix} - \begin{bmatrix} x_{av} \\ y_{av} \end{bmatrix}$$

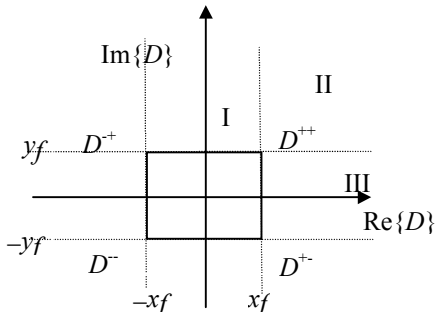

Fig. 2 The transformed Kharitonov rectangle.

The transformed region has as its origin the center of the Kharitonov rectangle as shown in Figure 2. Only the three regions where x and y are both positive need be considered because of the symmetry resulting from the transformation. For each point (x, y) on a boundary, symmetry yields the set of boundary points $\{(x,y), (-x,y), (x,-y), (-x,-y)\}$. Transforming back to the original coordinates, we have the four points $\{(-x-x_{av},-y-y_{av}), (x-x_{av},-y-y_{av}), (-x-x_{av},y-y_{av}), (x-x_{av},y-y_{av})\}$.

Theorem 1. Given a rectangular region $D^{\square}$ and a test point (x, y), the farthest point $(\hat{x}, \hat{y})$ in $D^{\square}$ to (x, y) and the closest point $(\breve{x}, \breve{y})$ in $D^{\square}$ to (x, y) are as given in Table 1.

Table 1. Closest and Farthest Points for the Transformed Domain.

Region	$(\breve{x}, \breve{y})$	$(\hat{x}, \hat{y})$
I	(x, y_f)	$(-x_f,-y_f)$
II	(x_f, y_f)	$(-x_f,-y_f)$
III	(x_f, y)	$(-x_f,-y_f)$

Proof: The distance $D^{\square}$ to (x, y) is maximized or minimized by separately maximizing $(x-\hat{x})^2$ and $(y-\hat{y})^2$ or minimizing $(x-\breve{x})^2$ and $(y-\breve{y})^2$, respectively. For the horizontal direction, $(x-\hat{x})^2$ is maximized at $\hat{x} = -x_f$. $(x-\breve{x})^2$ is minimized in II and III at $\breve{x} = x_f$. In Region I a minimum value of zero is possible with $\breve{x} = x$. The vertical distances can be similarly obtained to complete Table 1. ■

For each region the tracking bound is defined by

$$R^2 = \frac{(x-\hat{x})^2 + (y-\hat{y})^2}{(x-\breve{x})^2 + (y-\breve{y})^2} \le B^2 \tag{16}$$

with $B > 1$. At the boundary in Region II, we have

$$\begin{aligned} &(B^2-1)x^2 - 2x(B^2\breve{x} - \hat{x}) + (B^2\breve{x}^2 - \hat{x}^2) \\ &+ (B^2-1)y^2 - 2y(B^2\breve{y} - \hat{y}) + (B^2\breve{y}^2 - \hat{y}^2) = 0 \end{aligned} \tag{17}$$

with the permissible region outside the boundary. Completing the squares gives the equation of the circle with center (c_x, c_y) and radius c_r

$$(x-c_x)^2 + (y-c_y)^2 = c_r^2 \tag{18}$$

$$c_x = (B^2\breve{x} - \hat{x})/(B^2-1), c_y = (B^2\breve{y} - \hat{y})/(B^2-1)$$

$$c_r = \frac{B}{B^2-1}\sqrt{(\hat{x}-\breve{x})^2 + (\hat{y}-\breve{y})^2} \tag{19}$$

In Regions I and III, one quadratic term in the denominator vanishes. For Region I, (17) becomes

$$(B^2-1)y^2 - 2y(B^2\breve{y} - \hat{y}) - (x-\hat{x})^2 + (B^2\breve{y}^2 - \hat{y}^2) = 0 \tag{20}$$

Completing the squares we have the hyperbola

$$-\frac{(x-\hat{x})^2}{c_{ry}^2(B^2-1)} + \frac{(y-c_y)^2}{c_{ry}^2} = 1 \tag{21}$$

where $c_{ry} = B|\breve{y} - \hat{y}|/(B^2-1) = c_r$ with the x-related terms removed. The hyperbola is symmetric about axes through $(\hat{x}, c_y)$ with x-intercept at $\hat{x} \pm \sqrt{c_{ry}^2(B^2-1)}$ with asymptotes through $(\hat{x}, c_y)$ and $c_y \pm c_{ry}$. In Region III, we have similar hyperbolas with x and y interchanged and $c_{rx} = B|\hat{x} - \breve{x}|/(B^2-1) = c_r$ with the y-related terms removed.

Each boundary is valid only for the region for which the points $(\hat{x}, \hat{y})$ and $(\breve{x}, \breve{y})$ apply. In Region II, compensation is allowed outside the circle where the ratio is less than the specified value. In the remaining regions, the allowable compensation is outside the hyperbolas.

From (9) or (11), we obtain a boundary by replacing the inequality with an equality

$$(x-\breve{x})^2 + (y-\breve{y})^2 = (N/M_{lp})^2 \tag{22}$$

where M_{lp} denotes either the upper bound M_p or the lower bound M_l. The boundary is a circle of center $(\breve{x}, \breve{y})$ and radius N/M_{lp}. The allowable region is outside the circle.

The actuator bound is due to the maximum allowable compensation magnitude γ_{max} at each frequency. It is defined by the equation

$$x^2 + y^2 \le \gamma_{max}^2 \tag{23}$$

This boundary is a circle centered at the origin with radius γ_{max}, and the allowable region is inside the circle.

Theorem 2. Let the points $(\hat{x}, \hat{y})$ and $(\check{x}, \check{y})$ be known for a system with fixed numerator and interval denominator polynomial. The compensation boundaries and permissible regions are given by

1) In Region II, the tracking boundary is a circle of radius c_r centered at $(-c_x,-c_y)$ with the permissible region outside the boundary. In Region I, the tracking boundary is a hyperbola symmetric with respect to axes through $(-\hat{x},-c_y)$ with horizontal intercept at $-\hat{x}\pm\sqrt{B^2-1}$ and asymptotes through $(-\hat{x},-c_y)$ and $-c_y \pm c_{ry}$. In Region III, the tracking boundary is a hyperbola symmetric with respect to axes through $(-c_x,-\check{y})$ with horizontal intercept at $-\check{y}\pm\sqrt{B^2-1}$ and asymptotes through $(-c_x,-\check{y})$ and $-c_x \pm c_{rx}$.
2) The upper or lower boundary is a circle of radius N/M_{lp} centered at $(-\check{x},-\check{y})$ with the permissible region outside the boundary.
3) The actuator boundary is a circle of radius γ_{max} centered at the origin with the permissible region inside the boundary.

Proof: The results are obtained on replacing (x,y) by $(-x,-y)$ in (16), (17), (18). ■

Remark 1: Theorem 2 is valid only if we fix the farthest and closest points in the Kharitonov rectangle to a test point. In Regions I and II this is not the case. The result is that the robust stability boundaries in these regions are actually *straight lines* parallel to the adjacent edge of Kharitonov rectangle and tangent to the set of circles for the region.

We assume that we remain in a single region so that the points for maximum and minimum distances are fixed to derive the following monotonicity properties.

Theorem 3. The function (1) is monotone increasing in Region I or III and is unimodal in Region II.

Proof: Differentiate the rational function of (16) and equate to zero to obtain the minima and maxima. For Region I, $\check{x} = x$ and $\hat{x} = -x_f$, so that (16) reduces to

$$R^2 = \frac{(x+x_f)^2 + (y+y_f)^2}{(y-y_f)^2} \le B^2$$

Differentiating w.r.t. x and equating to zero gives

$$\tfrac{1}{2}\frac{\partial R^2}{\partial x} = \frac{x+x_f}{(y-y_f)^2} = 0$$

This indicates a positive derivative with the inadmissible negative root $x=-x_f$. Differentiating with respect to y and equating to zero, we obtain

$$\tfrac{1}{2}\frac{\partial R^2}{\partial y} = \frac{(y+y_f)(y-y_f) - \left[(y+y_f)^2 + (x+x_f)^2\right]}{(y-y_f)^3} = 0$$

$$(x+x_f)^2 + 2y_f(y+y_f) = 0$$

This indicates a positive derivative with the inadmissible negative root

$$y = -y_f - (x+x_f)^2 / (2y_f)$$

Because the derivatives are positive and have no positive real roots we conclude that the function is montone increasing.

Interchanging x and y, we prove monotonicity in Region III. In Region II, $\check{x} = x_f$ and $\hat{x} = -x_f$, so that (16) becomes:

$$R^2 = \frac{(x+x_f)^2 + (y+y_f)^2}{(x-x_f)^2 + (y-y_f)^2} \le B^2$$

$$\tfrac{1}{2}\frac{\partial R^2}{\partial x} = \frac{-2x_f(x^2 - x_f^2) - 4yy_f x + 2x_f\left[y^2 + y_f^2\right]}{\left[(x-x_f)^2 + (y-y_f)^2\right]^2} = 0$$

This yields the roots

$$x = -(yy_f/x_f) \pm \sqrt{(yy_f/x_f)^2 + y^2 + y_f^2 + x_f^2}$$

One root is negative and is therefore inadmissible. The second root is greater than x_f and is therefore inside Region II. Therefore, the function is unimodal in Region II. For large x the function approaches its minimum value of unity. We conclude that in Region II, the inadmissible region is in the vicinity of a maximum of the ratio R^2 as shown in Figure 3. Because the value of R^2 as $x \to x_f$ may be larger than B^2, the intersection of the curve of Figure 3 with the $R^2 = B^2$ line may occur at *one or two points*. ■

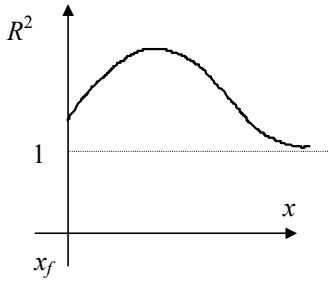

Fig. 3 Unimodal function in Region II.

The coordinate transformation is linear, and the boundaries retain their form. However, the transformation reveals the following regarding the stability robustness boundary of Theorem 2.

Theorem 4. The upper and lower frequency response boundaries for the transformed domain in Regions I and III are straight lines parallel to the edges of the

Kharitonov rectangle. In Region II, the boundary is a circle of radius N/M_{lp} centered at (x_f, y_f).

Proof: The upper (stability robustness) or lower boundary is given by (22) with $(\breve{x}, \breve{y})$ defined for Regions I, II, III. In Region I, $(\breve{x}, \breve{y}) = (x, y_f)$, and the boundary is the vertical line $y = y_f + N/M_{lp}$. Similarly, in Region III, the boundary is the vertical line $x = x_f + N/M_{lp}$. In Region II, $(\breve{x}, \breve{y}) = (x_f, y_f)$, and the boundary is the circle $(y - y_f)^2 + (x - x_f)^2 = (N/M_{lp})^2$ ■

Remark 2: Transforming the rectangle using the inverse transformation of (22) gives a second rectangle centered at $(-x_{av}, -y_{av})$ with the symmetric boundaries about the rectangle. Hence, the boundaries and the permissible compensation can be plotted easily.

Remark 3: For fixed numerator and affine denominator uncertainty structure, the denominator value set is a polygon. The upper and lower frequency response boundaries are made up of edges parallel to the edges of the polygon and circular arcs around the vertices. For a multiaffine denominator, the convex hull of the value set is a polygon [7], and a somewhat conservative robust stability bound can be explicitly obtained.

IV. Algorithm for Feasible Compensation Region

We now state the main algorithmic result of this paper. In (2) let the order of the numerator polynomial N be m and the order of the uncertain denominator polynomial D be n. Horner's Rule evaluates these polynomials in time $\theta(m)$ *resp.* $\theta(n)$ ([8], ex. 1.2-4). The numerator need be evaluated only once, but in order to compute the Kharitonov rectangle, the denominator is recomputed (in optimal time $\theta(n)$) for each of n_w sample frequencies ω. For fixed ω, Theorem 2 prescribes how to determine, in optimal time $\theta(1)$, a set of constraints defining the feasible region of compensation. Thus, in time $\theta(n_w n+m)$, the frequency-divided boundary of minimum magnitude compensations can be computed. When, as is often the case, $n_w\, n$ is much greater than m, the running time is $\theta(n_w\, n)$. This compares favorably with the $\theta(n_w\, n_\gamma\, n_\phi\, n)$ running time of [6] and is certainly preferable to the $\theta(n_q\, n_w\, n_\gamma\, n_\phi\, n)$ running time of the traditional gridding approach [9], where n_q is the total number of grid points in the uncertain parallelepiped Q, n_γ is the number of grid points along the axis of compensation magnitude, and n_ϕ is the number of points along the compensation phase axis. Since the numerator need be evaluated only once, the Rule of Products implies that the search as described runs in time $\theta(n_q n_w n_\gamma n_\phi n+m)$.

To demonstrate the reduction in computational time achieved here, we examine the case of a plant transfer function with six uncertain parameters and ten grid points for each parameter $n_q=10^6$. For $n_\gamma = n_\phi = 10$, the overall reduction achieved here is by a factor of one hundred relative to [6] and 10^8 relative to the gridding method!

In the next section, we discuss two simple examples to illustrate our computational approach to bound determination. We purposefully avoid more complex examples that would obscure the design procedure.

V. Examples

Example 1: Position Control System

Consider the position control system with motor and load transfer function $G(s) = 10/[s(\tau s + 1)]$, where $\tau \in [8, 12]$. The product of the numerator of the transfer function and the compensator K is $C = 10K$. The denominator is an interval polynomial whose value set is the interval $[-8\omega^2, -12\omega^2]$ on the straight line parallel to the real axis with imaginary intercept ω. Here, the twelve regions of Figure 2 reduce to 6 and the three regions of Figure 4 reduce to two. The bounds for the system are shown in Figure 5 together with the value set for ω=1rad/s.

For this example, c_{ry} is zero and the hyperbolas for Region I, reduce to a single point outside the respective region. Region III, are not defined and need not be considered. In Region II, the tracking boundaries are circular arcs with the permissible region outside the arcs. The stability robustness boundary comprises circular arcs of radius $N/M_p = 5$ and straight lines parallel to the value set. The actuator bound is a circle of radius γ_{act}. The feasible compensation region is inside the actuator boundary and outside both the tracking boundary and the stability robustness boundary.

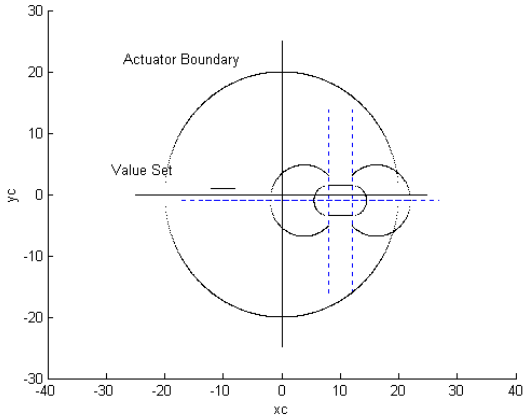

Fig. 5 Boundaries for position control system.

Example 2: Two-Parameter Uncertainty

Consider the transfer function $G(s) = 1/[a_2 s^2 + a_1 s + 1]$ where $a_i \in [a_i^-, a_i^+]$, $i = 1, 2$. For $G(j\omega)$, the x and y coordinates of the denominator are in the ranges $x \in [1 - a_2^+\omega^2, 1 - a_2^-\omega^2], y \in [a_1^-\omega, a_1^+\omega]$. The QFT

bounds are shown in Figure 4. The permissible region is inside the circle of the actuator bound, outside the tracking bounds made up of hyperbolic and circular segments and outside the robust stability bounds. We select a design point for each point on a frequency grid. We then fit the set of design points with a compensator. Finally, we check the compensated system to determine if all design constraints are satisfied. We can also add the bounds of the form (10) to Figure 4 so that the designer can attempt to satisfy all design constraints with a single compensator. If successful, the added cost of a prefilter can be avoided. If not, we ignore the additional bound and design a loop compensator. We then add a prefilter to achieve the desired performance.

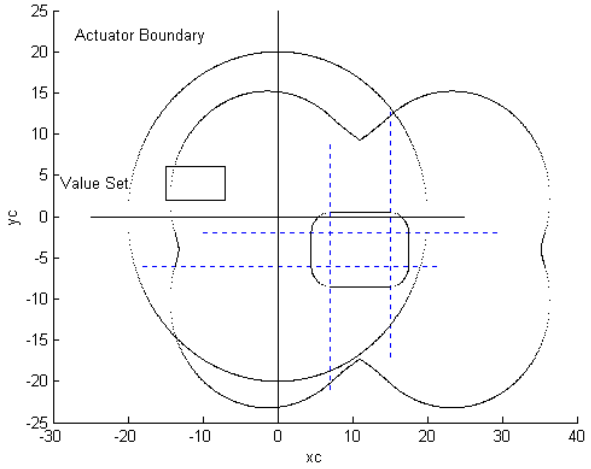

Fig. 4 QFT boundaries for the two-parameter system.

V. Conclusion

The simple case considered in this paper demonstrates the considerable savings possible in the computation of QFT bounds using value sets, coordinate transformations, and subdivision of the compensator plane. For a region where the farthest and closest points in the value set to a test point are determined, closed form expressions for the boundaries are obtained. This allows the computation of the compensation bounds in time $\theta(n_w n)$.

For a system with a more complex denominator structure, the upper (robust stability) bound and the lower bound can be calculated as outlined in Remark 3. These problems will be examined by the authors in more detail in future work. However, it may be difficult to extend the results obtained here to tracking bounds expressed as a ratio of maximum to minimum frequency response. This further justifies the move by QFT researchers [4] to abandon ratio tracking bounds and specify tracking using an upper and lower bound to simplify the design procedure and improve its computational efficiency.

References

[1] J. J. D'Azzo & C. H. Houpis (1988). *Linear Control System Analysis and Design*. McGraw-Hill Book Company, New York.

[2] C. Borghesani, C., Y. Chait & O. Yaniv (1994). *Quantitative feedback theory toolbox*. The Mathworks Inc., Natick, MA.

[3] M. Brown & I. R. Peterson (1991). Exact computation for the Horowitz bound for interval plants. *30th CDC*, Brighton, England, pp. 2268-2273.

[4] G. M. Rodriguez, Y. Chait & C. V. Hollot (1995). A new algorithm for computing QFT bounds. *Proc. 1995 ACC*, Seattle, WA.

[5] L. Longdon & D. J. East (1979). A simple geometrical technique for determining loop frequency response bounds which achieve prescribed sensitivity specifications. *Int. J. Control*, **30**, pp. 153-158.

[6] M. S. Fadali & L. E. LaForge, Algorithmic Analysis of Geometrically Computed QFT Bounds, *Proc. 1996 IFAC World Congress*, Vol. H, pp. 297-302. San Francisco, CA, June, 1996.

[7] M. S. Fadali and L. E. LaForge (2001). Linear time computation of feasible regions for robust Compensators, *J. Robust and Nonlinear Control*, **11**, pp. 819-856.

[8] B. K. Barmish, (1994). *New Tools for Robustness of Linear Systems*. Macmillan, NY, NY.

[9] T. H. Cormen, C. E. Leiserson & R. L. Rivest (1993). *Introduction to Algorithms*. McGraw Hill, NY, NY.

[10] El-Zayyat, K.(1994). *VSC/QFT Robust Design of Systems with Bounded Uncertainties*, Ph.D. Dissert., (M. S. Fadali, Advisor), UNR, Reno, NV.